NANO MICRO small

Supporting Information

for *Small,* DOI: 10.1002/smll.202300606

MOF-Derived In_2O_3/CuO p-n Heterojunction Photoanode Incorporating Graphene Nanoribbons for Solar Hydrogen Generation

Li Shi, Daniele Benetti, Qin Wei,* and Federico Rosei**

Supporting Information

MOF-derived In_2O_3/CuO p-n heterojunction photoanode incorporating graphene nanoribbon for solar hydrogen generation

Li Shi[a,b], Daniele Benetti[a,*], Qin Wei[b,*], and Federico Rosei[a,*]

[a] *Centre for Energy, Materials and Telecommunications, Institut National de la Recherche Scientifique, 1650 Boul. Lionel-Boulet, Varennes, QC J3X1S2, Canada*

[b] *Key Laboratory of Interfacial Reaction & Sensing Analysis in Universities of Shandong, School of Chemistry and Chemical Engineering, University of Jinan, Jinan 250022, PR China*

* Corresponding author: daniele.benetti@inrs.ca (D.B.); chm_weiq@ujn.edu.cn (Q.W.); federico.rosei@inrs.ca (F.R.)

A Table of Contents

1. TGA curves of the as-obtained MIL-68(In), Cu-BDC, and MIL-68(In)/Cu-BDC……..……..……page 1

2. SEM images of MIL-68(In), XRD of MIL-68(In), and Cu-BDC……..……page 2

3. SEM images of In_2O_3/CuO after annealing MIL-68(In)/Cu-BDC…….……page 3

4. TEM and SAED images of In_2O_3 and CuO……....page 4

5. EDX spectrum of In_2O_3/CuO……..……page 5

6. UV-DRS spectra and Tacu plot of CuO, In_2O_3, and In_2O_3/CuO composite.…...page 6

7. UPS spectrum of CuO, In_2O_3, and In_2O_3/CuO composite……..…page 7

8. XPS spectra of pure CuO, In_2O_3, core level, and valence spectra of different samples……...page 8

9. Determination of the band positions in the photocatalysts……..……..page 9

10. Mott-Schottky plot of CuO, In_2O_3, and In_2O_3/CuO composite…....……..page 11

11. Raman spectra of GNRs, In_2O_3/CuO, and In_2O_3/CuO-GNRs hybrid……..page 12

12. Plain-view, cross-sectional SEM image, and EDS mapping of In_2O_3/CuO-GNRs photoanode……..……..……...….……page 13

13. Photocurrent density of In_2O_3 and In_2O_3-0.03wt GNRs……..……..…page 14

14. TEM images of the In_2O_3/CuO-0.03wt GNRs after the stability test……page 15

15. Online gas chromatography to measure the H_2 evolution……...……page 16

16. The values of the R_{CT}……..……..…….....page 18

17. Summary of the performance of In_2O_3-based photoanode…….....page 19

18. References…….....page 20

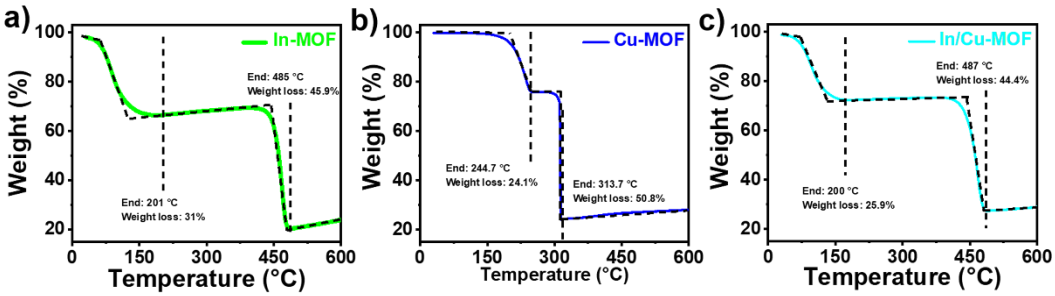

Figure S1. TGA curves of the as-obtained (a) MIL-68(In), (b) Cu-BDC, and (c) MIL-68(In)/Cu-BDC

As shown in the TGA curve in Figure S1a, the weight loss of MIL-68(In) from room temperature to 200 °C (approximately 31.2 wt%) can be attributed to the removal of physically adsorbed gases, moisture, and DMF solvent. A further significant weight loss (approximately 45.9 wt%) between 400 and 485 °C is instead attributed to the decomposition of the MOF skeleton.

For the Cu-BDC part, the weight loss around 24.1 wt% from room temperature to 244 °C could be attributed to the removal of the physically adsorbed gases, moisture, and DMF solvent, whereas the noteworthy weight loss (around 50.8 wt%) from temperature 370 °C to 313 °C is assigned to the decomposition of the MOF skeleton (Figure. S1b).

On the basis of the TGA results, the pyrolysis temperature for MIL-68(In) and Cu-BDC precursor was set to 500 °C and 350 °C, respectively, with a heating rate of 5 °C min^{-1} for 1 h in air atmosphere.

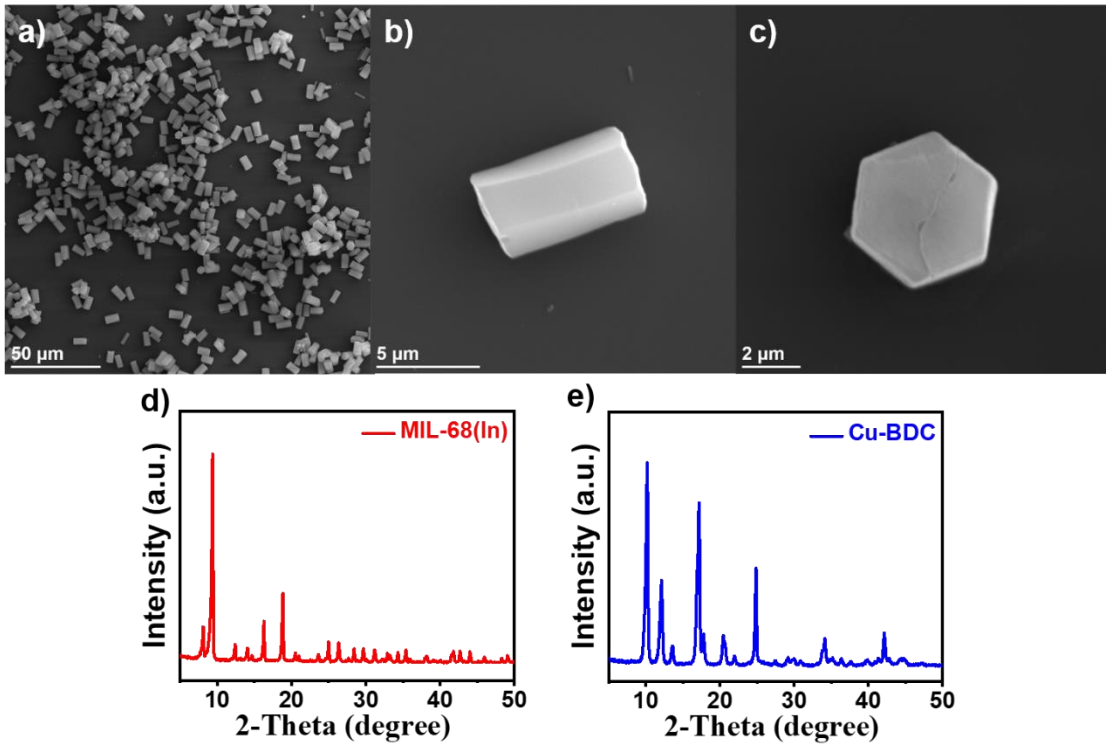

Figure S2. SEM images of MIL-68(In)(a-c), XRD of (d) MIL-68(In), and (e) Cu-BDC.

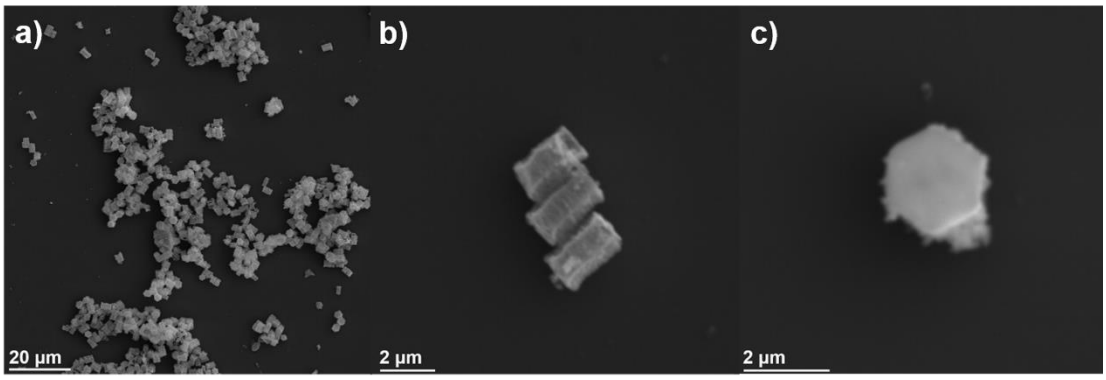

Figure S3. SEM images of In_2O_3/CuO after annealing MIL-68(In)/Cu-BDC.

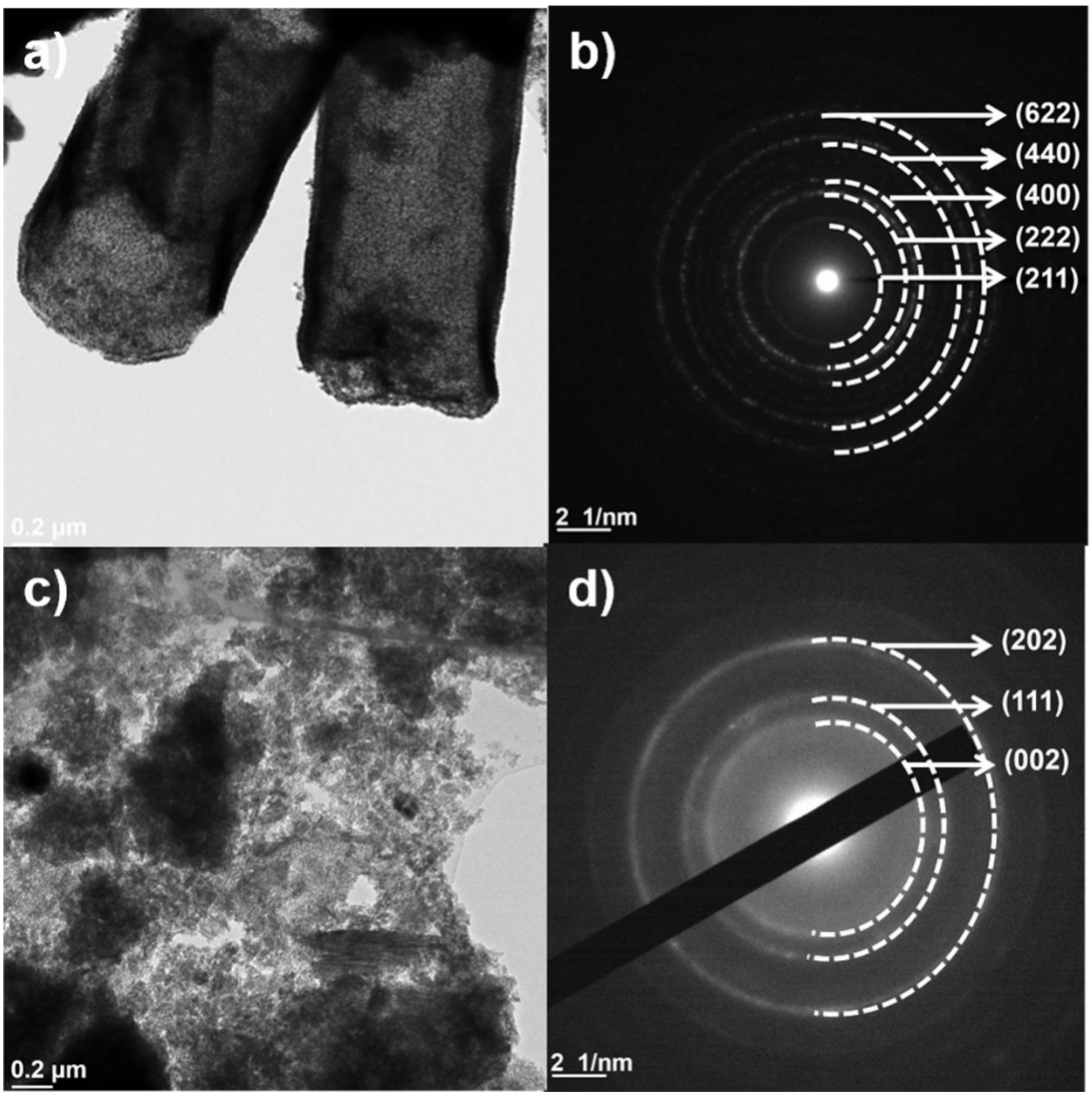

Figure S4. TEM and SAED images of (a, b) In_2O_3 from MIL-68(In) and (c, d) CuO from Cu-BDC.

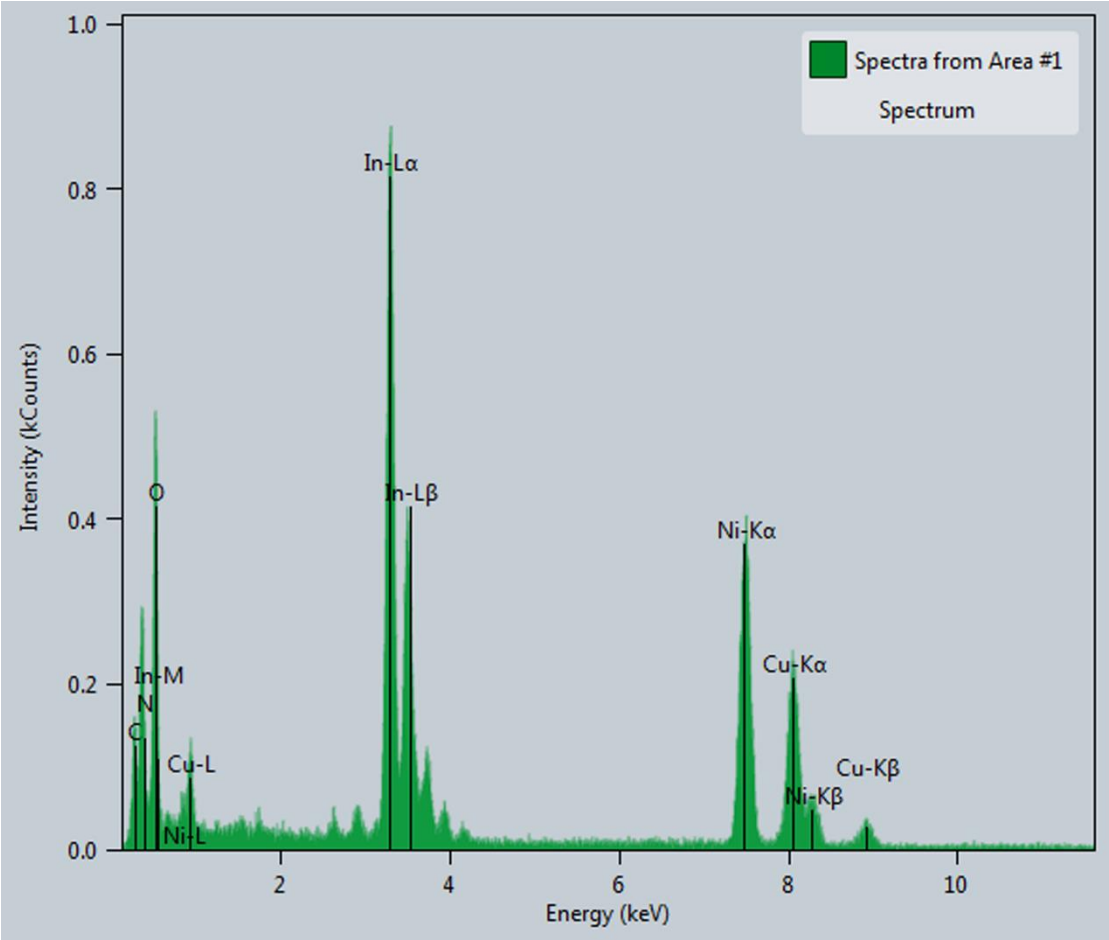

Figure S5. EDX spectrum of In_2O_3/CuO (Ni substrate).

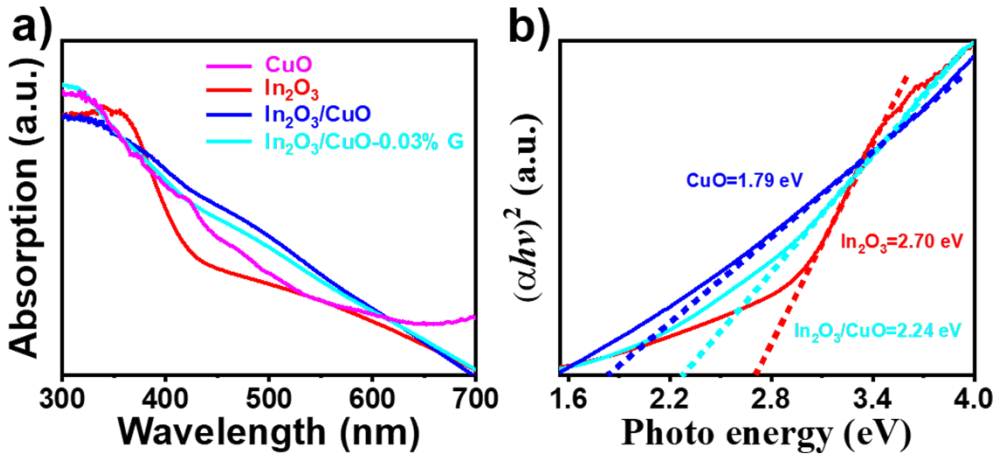

Figure S6. (a) UV-DRS spectra of CuO, In_2O_3, In_2O_3/CuO composite and In_2O_3/CuO-0.03 wt% GNRs. (b) The extrapolation of Tauc plots $((\alpha h\nu)^2$ versus photon energy ($h\nu$)) for CuO, In_2O_3, and In_2O_3/CuO composite.

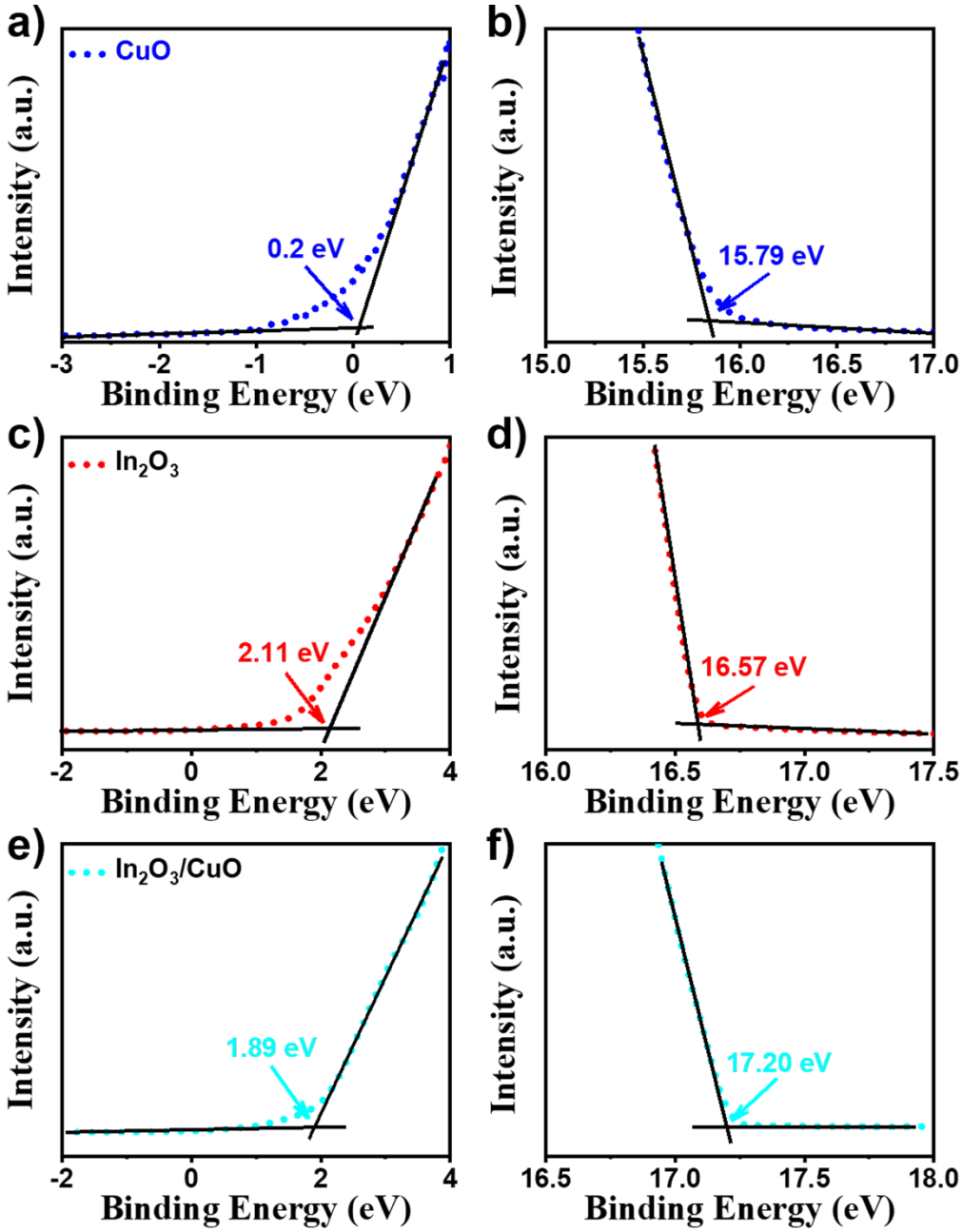

Figure S7. High binding energy cut-off (a) and low binding energy cut-off (b) of UPS spectra of CuO, In_2O_3, and In_2O_3/CuO composite.

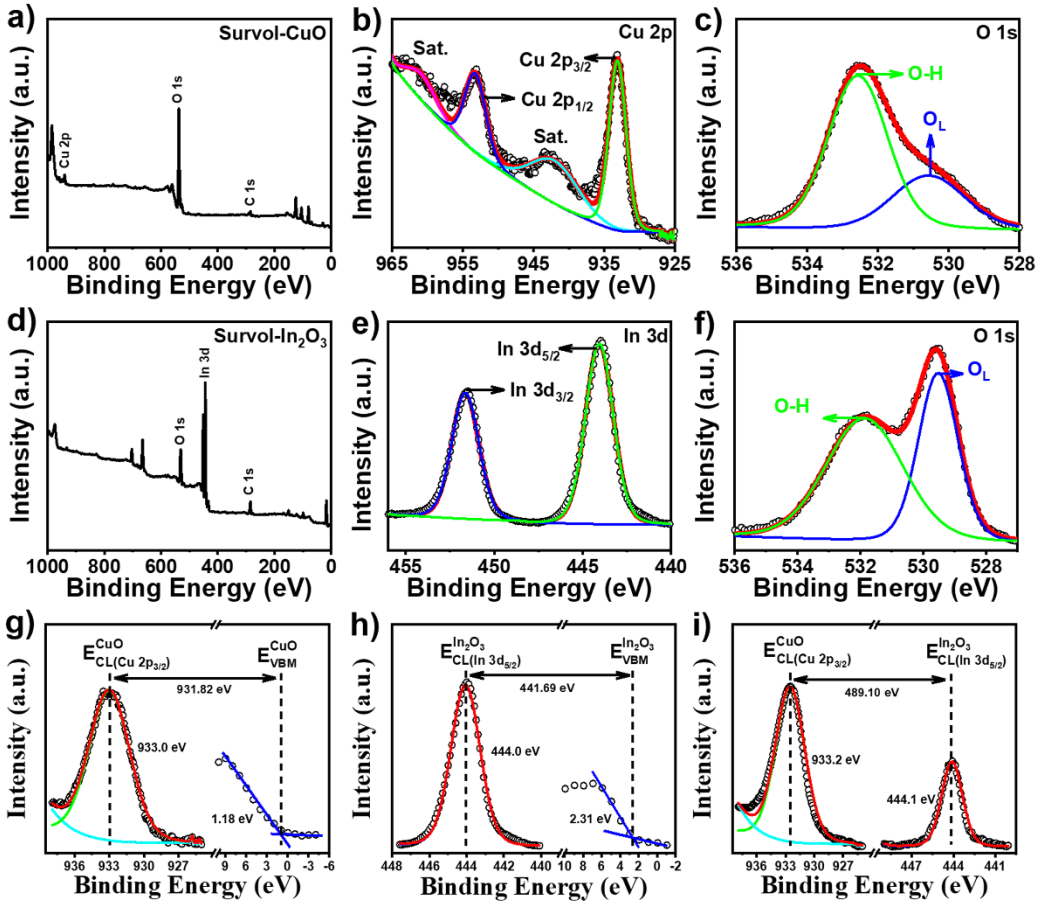

Figure S8. XPS survey spectra of (a) CuO. High resolution Cu 2p spectra (b). High resolution O1s spectra of CuO (c). Survol spectra of (d) In_2O_3. High resolution In 3d spectra (e). High resolution O1s spectra (f). XPS core level and valence spectra from (g) CuO from Cu-BDC, (h) In_2O_3 from MIL-68(In) and (i) In_2O_3/CuO composite.

Construction of energy diagram

In order to build the band diagram of pure materials (before contact) and the composite from UPS data, the position of the valence band maximum is obtained from Eq. (S1):

$$E_{VB} = E_F - X\ (S1)$$

Where E_F is the energy of the Fermi level and X is obtained from the extrapolation of the onsets in the UPS spectrum [X(CuO) = 0.2 eV, X(In_2O_3) = 2.11 eV, and X(In_2O_3/CuO) = 1.89 eV].

The Fermi level needed in Eq. (S1) is equivalent to the negative value for the work function (E_F = -Φ), and can be calculated using Eq. (S2):

$$\Phi = 21.21\ eV - E_{SO}\ (S2)$$

In Eq. (2) He I radiation (21.21 eV) is used to estimate the E_F and E_{SO} is the secondary electron onset, which is obtained from the linear extrapolation of the UPS spectrum indicated above.

[E_{SO}(CuO), E_{SO}(In_2O_3), and E_{SO}(In_2O_3/CuO) are 15.79 eV, 16.56 eV, and 17.2 eV].

Thus, the Φ of them could be obtained [Φ (CuO), Φ (In_2O_3), and Φ (In_2O_3/CuO) are 5.42 eV, 4.64 eV, and 4.01 eV]. (e.g., Φ(CuO) = 21.21 eV - E_{SO}(CuO) = 21.21 eV - 15.79 eV = 5.42 eV)

Moreover, based on the Eq (E_F = -Φ), their E_F are [E_F(CuO), E_F(In_2O_3), and E_F(In_2O_3/CuO) are -5.42 eV, -4.64 eV, and -4.01 eV].

According to the Eq S1, we could further get the E_{VBM} of them, which are [E_{VBM}(CuO) = -5.62 eV, E_{VBM}(In_2O_3) =-6.75 eV, and E_{VBM} (In_2O_3/CuO) = -5.90 eV]. (e.g., E_{VBM}(CuO) = E_F(CuO) - X = -5.42 eV-0.2 eV = -5.62 eV).

Then, the conduction band minimum potential can be readily calculated applying Eq. (S3):

$$E_{CB} = E_F + E_{BG} - X\ (S3)$$

where the bandgap energy E_{BG} is obtained by DRS measurements. [E_{BG}(CuO), E_{BG}(In_2O_3), and E_{BG}(In_2O_3/CuO) are 1.79 eV, 2.70 eV and 2.24 eV]. Their E_{CBM} are [E_{CBM}(CuO) = -3.83 eV, E_{CBM}(In_2O_3) =-4.05 eV, and E_{CBM} (In_2O_3/CuO) = -3.66 eV] (e.g., E_{CBM}(CuO) = E_F(CuO) + E_{BG}(CuO) - X = -5.42 eV + 1.79 eV -0.2 eV=-3.83 eV).

In the last, all the data could be transfer to NHE by Eq (E_{abs} = -E^{Θ}- 4.44).

1. [E_F(CuO) = 0.98 eV, E_F(In_2O_3) = 0.2 eV, and E_F(In_2O_3/CuO) = -0.43 eV] (e.g.,

$E_F(CuO) = -E^{\Theta}$- 4.44, $E^{\Theta}(\underline{E_F(CuO)})$ = 5.42 eV - 4.44 eV = 0.98 eV);

2. [$\underline{E_{VBM}(CuO) = 1.18\ eV}$, $\underline{E_{VBM}(In_2O_3) = 2.31\ eV}$, and $\underline{E_{VBM}\ (In_2O_3/CuO) = 1.46\ eV}$] (e.g., $E_{VBM}(CuO) = -E^{\Theta}$- 4.44, $E^{\Theta}(\underline{E_{VBM}(CuO)})$ = 5.62 eV - 4.44 eV = 1.18 eV);

3. [$\underline{E_{CBM}(CuO) = -0.61\ eV}$, $\underline{E_{CBM}(In_2O_3) = -0.39\ eV}$, and $\underline{E_{CBM}\ (In_2O_3/CuO) = -0.78\ eV}$] (e.g., $E_{CBM}(CuO) = -E^{\Theta}$- 4.44, $E^{\Theta}(\underline{E_{VBM}(CuO)})$ = 3.83 eV - 4.44 eV = -0.61 eV).

The results are summarized in the Table 1.

As mentioned in the manuscript, The valence band offset (ΔE_{VBO}) and conduction band offset (ΔE_{CBO}) could be obtained via Eq (1), Eq (2), and Eq (3).

$$\Delta E_{VBO} = (E_{CL}^{CuO} - E_{VBM}^{CuO}) - \left(E_{CL}^{In_2O_3} - E_{VBM}^{In_2O_3}\right) - \Delta E_{CL}^{Int} \quad (1)$$

$$\Delta E_{CL}^{Int} = (E_{CL}^{CuO} - E_{CL}^{In_2O_3})^{In_2O_3/CuO} \quad (2)$$

$$\Delta E_{CBO} = E_{BG}^{CuO} - E_{BG}^{In_2O_3} + \Delta E_{VBO} \quad (3)$$

Therefore, the energy difference between the core level (E_{CL}) and the valence band maximum (E_{VBM}) in the pure materials are shown in the Figure S8g-i.

$$\begin{aligned} \Delta E_{VBO} &= (E_{CL}^{CuO} - E_{VBM}^{CuO}) - \left(E_{CL}^{In_2O_3} - E_{VBM}^{In_2O_3}\right) - \Delta E_{CL}^{Int} \\ &= (933.0\ eV - 1.18\ \text{eV}) - (444.0\ eV - 2.31\ \text{eV}) - 489.10\ \text{eV} \\ &= 1.03\ \text{eV} \end{aligned}$$

$$\Delta E_{CL}^{Int} = (E_{CL}^{CuO} - E_{CL}^{In_2O_3})^{In_2O_3/CuO} = (933.2\ eV - 444.1\ \text{eV})^{In_2O_3/CuO} = 489.10\ eV$$

$$\Delta E_{CBO} = E_{BG}^{CuO} - E_{BG}^{In_2O_3} + \Delta E_{VBO} = 1.79\ eV - 2.70\ eV + 1.03\ eV = 0.12\ eV$$

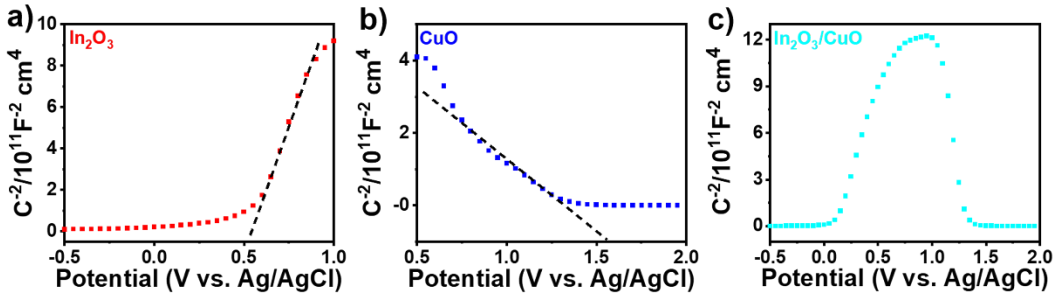

Figure S9. Mott-Schottky plot of CuO, In_2O_3, and In_2O_3/CuO composite.

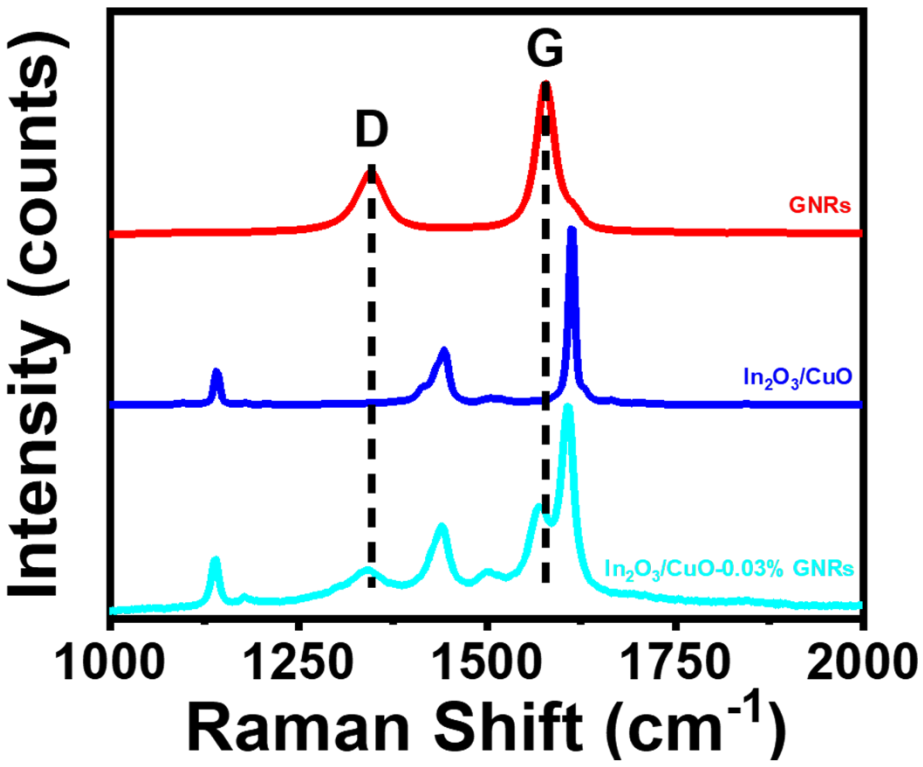

Figure S10. Raman spectra of bare GNRs (red line), In_2O_3/CuO composite (blue line), and In_2O_3/CuO-GNRs hybrid mesoporous film (cyan line).

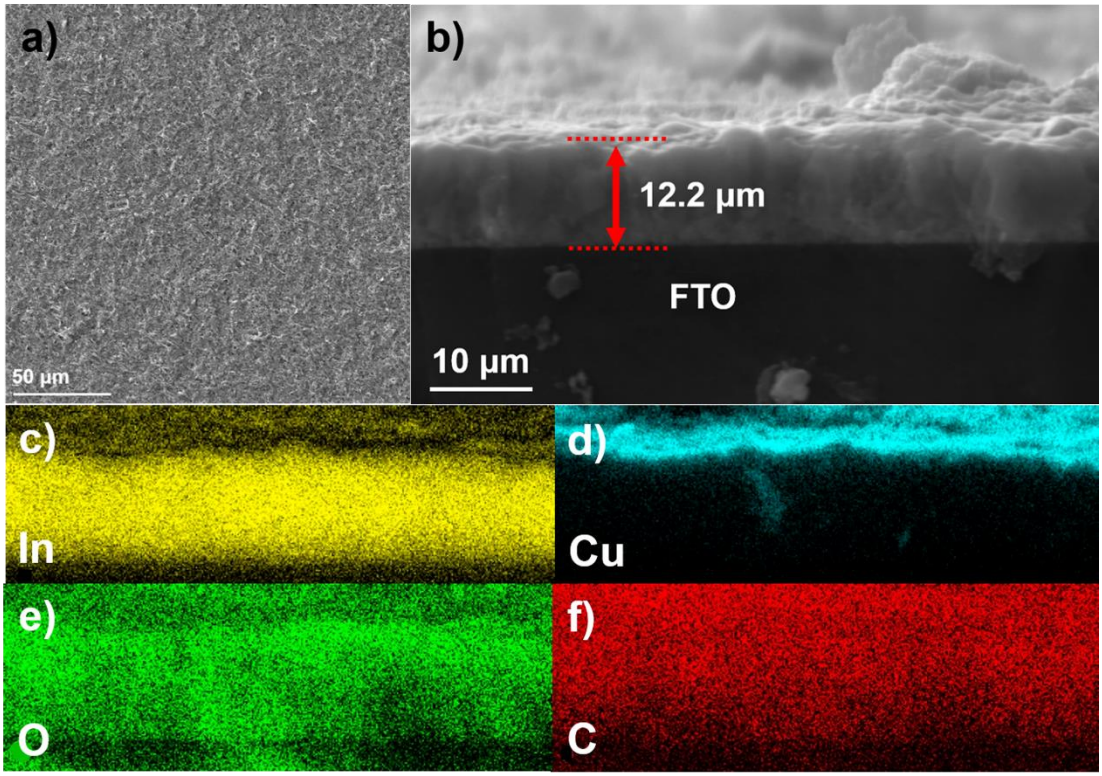

Figure S11. plain-view and cross-sectional SEM image of In_2O_3/CuO-0.03 wt% GNRs (a and b); EDS mapping analysis of all the elements in relevant In_2O_3/CuO-0.03 wt% GNRs electrode including (c) In, (d) Cu, (e) O, and (f) C.

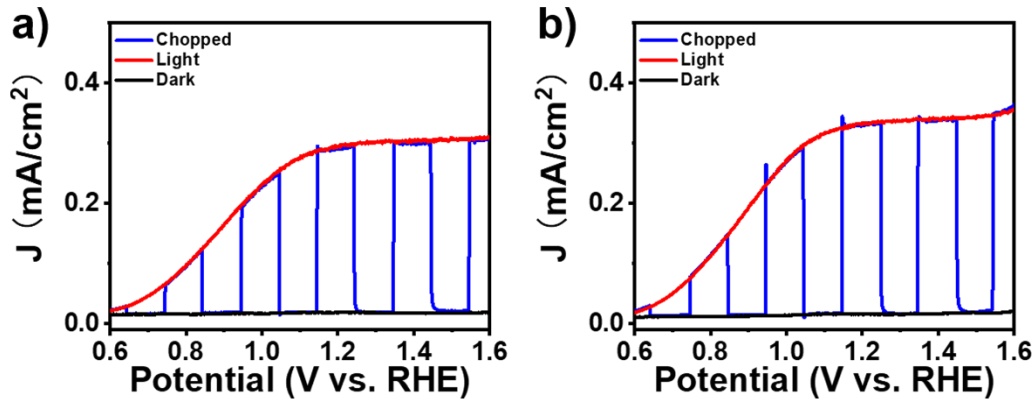

Figure S12. Photocurrent density of (a) In_2O_3 and (b) In_2O_3-0.03wt GNRs.

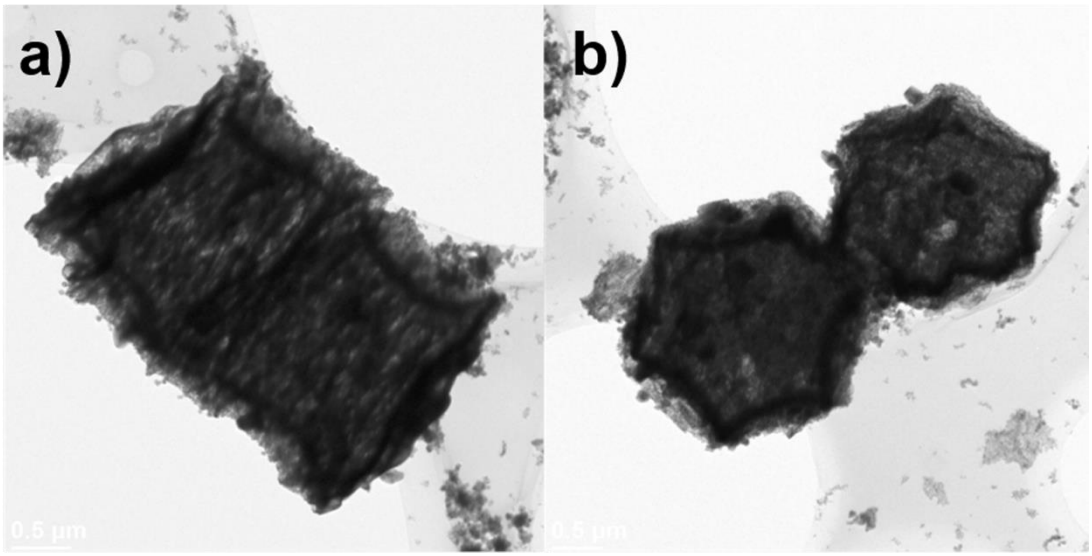

Figure S13. TEM images of the In_2O_3/CuO-0.03wt GNRs after the stability test from different directions.

Online gas chromatography to measure the H_2 evolution:

A gas-tight cell (total volume: 50 mL) was used for online gas chromatography (GC) and it was filled with 30 mL electrolyte in a three-electrode cell configuration, using a In_2O_3/CuO-0.03 wt% GNRs photocathode as working electrode, an Ag/AgCl saturated reference electrode and a Pt plate as working electrode. Ar was used as carrier gas at a flow rate of 20 sccm and the electrolyte was continuously stirred. Before the measurements, the electrolyte was saturated with Ar gas for at least 60 minutes. A gas outlet was connected to a gas chromatograph (Perkin Elmer Clarus 580 GC) for periodical sampling. A thermal conductivity detector (TCD) was used for detecting H_2. A gas aliquot was automatically injected into the GC every 180 s. During the online GC, a chronoamperometric measurement was performed by applying a 1.4 V vs RHE potential for 1 h.

The theoretical number of moles of hydrogen evolved can be calculated from Faraday's 2nd law of electrolysis according to the following equation:

$$n_{H_2}(\text{theoretical}) = \frac{Q}{zF} = \frac{I \times t}{zF}$$

Where n_{H_2} is the number of moles of hydrogen produced, Q is the total charge passed during electrolysis, z is the number of electrons transferred during HER (i.e. z = 2), I is the applied current, t is the electrolysis time in seconds, and F is the Faraday constant 96 485.33 C mol^{-1}.

The Faradaic efficiency was calculated as follows:

$$\eta_{Faradaic} = \frac{n_{H_2}(\text{experimental})}{n_{H_2}(\text{theoretical})} \times 100\%$$

For example, according to gas chromatography after 5400s, the H_2 gas evolved was 7.947×10^{-6} mol, whereas the current obtained by chronoamperometry is 0.27 mA.

$$n_{H_2}(\text{theoretical}) = \frac{0.00027\ (A)\ \times\ 5400\ (s)}{2\ \times\ 96485.33\ C \cdot mol^{-1}} =\ 7.556\ \times\ 10^{-6}\ mol$$

Consequently,

$$\eta_{Faradaic} = \frac{7.556 \times 10^{-6}\, mol}{7.947 \times 10^{-6}\, mol} = 95.11\%$$

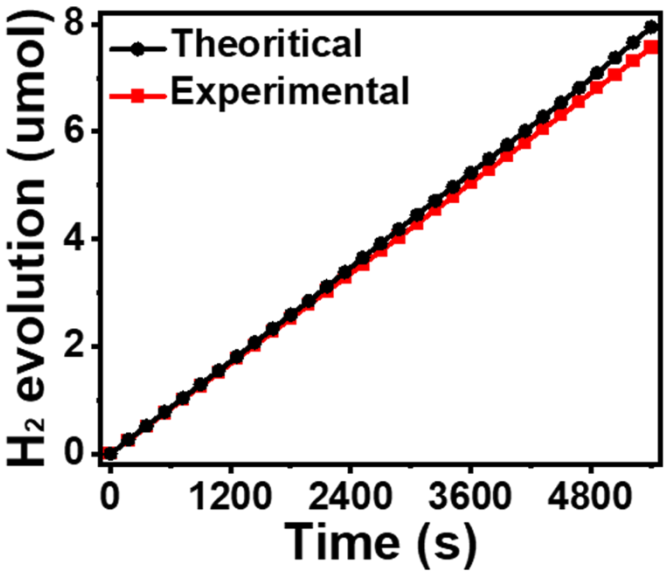

Figure S14. H_2 evolution of In_2O_3/CuO-0.03wt GNRs as a function of time at 1.4 V vs RHE under 100 mW/cm^2 illumination with AM 1.5 G filter. The evolution of H_2 exhibits a nearly linear increase over time (solid red curve). H_2 evolution is also calculated from the measured current (solid black curve).

Table S1 the values of the R_{CT}

Sample	R_{ct} (Ω)
CuO	6420
In_2O_3	4270
In_2O_3/CuO	622
In_2O_3/CuO-0.03 wt% GNRs	109

Table S2 Comparison of the PEC performance of some representative In_2O_3 photocatalysts with literature

Photocathode	Electrolyte	Light Source	Photocurrent density (mA cm^{-2})	Ref.
In_2O_3	**1 M NaOH**	**1 Sun**	**0.3 (1.6 V vs RHE)**	**Present work**
In_2O_3/CuO	**1 M NaOH**	**1 Sun**	**0.89 (1.6 V vs RHE)**	**Present work**
In_2O_3/CuO-0.03 wt% GNRs	**1 M NaOH**	**1 Sun**	**1.51 (1.6 V vs RHE)**	**Present work**
In_2O_3/TiO_2	0.1 M Na_2SO_4	350W Xe lamp	0.65 (No mention)	[1]
In_2S_3/CdS/NiOOH	0.25 M Na_2S and 0.35 M Na_2SO_3	1 Sun	1.01 (1.23 V vs RHE)	[2]
In_2O_3/In_2S_3	1 M NaOH	300W Xe lamp	0.53 (1.23 V vs RHE)	[3]
N-doped In_2O_3	0.1 M Na_2SO_4	300W Xe lamp	0.2 (1.6 V vs RHE)	[4]
In_2O_3/Fe_2O_3	0.1 M NaOH	300W Xe lamp	0.04 (1.6 V vs RHE)	[5]
In_2O_3/ZnO	0.5 M Na_2SO_4	300W Xe lamp	0.36 (0.5 V vs Ag/AgCl)	[6]
In_2O_3/Carbon	Triethanolamine (8 vol%)	300W Xe lamp	0.04 (0.2 V vs Hg/Hg_2Cl_2)	[7]

Supplementary references:

[1] H. Yang, J. Tian, Y. Bo, Y. Zhou, X. Wang, H. Cui, *J. Colloid Interface Sci.* **2017**, 487, 258.

[2] L. Wei, J. Zhang, M. Ruan, *Appl. Surf. Sci.* **2021**, 541, 148431.

[3] H. Xu, H. Chen, S. Chen, K. Wang, X. Wang, *Int. J. Hydrogen Energy* **2021**, 46, 32445.

[4] X. Gan, R. Zheng, T. Liu, J. Meng, R. Chen, X. Sun, X. Sun, *Chem. Eur. J.* **2017**, 23, 7264.

[5] L. Wu, S. Ma, J. Li, X. Li, *Thin Solid Films* **2021**, 724, 138600.

[6] F.-Y. Su, W.-D. Zhang, *Mater. Lett.* **2018**, 211, 65.

[7] R. Li, L. Sun, W. Zhan, Y.-A. Li, X. Wang, X. Han, *J. Mater. Chem. A* **2018**, 6, 15747.